Hindawi
Journal of Chemistry
Volume 2022, Article ID 1963973, 11 pages
https://doi.org/10.1155/2022/1963973

Research Article

Green Power Generation by Microbial Fuel Cells Using Pharmaceutical Wastewater as Substrate and Electroactive Biofilms (Bacteria/Biocarbon)

Ivonne L. Alonso-Lemus,[1] **Carlos Cobos-Reyes**,[2] **Mayra Figueroa-Torres**,[3] **Beatriz Escobar-Morales**,[4] **K. Kunhiraman Aruna**,[5] **Prabhu Akash**,[5] **Fabian Fernández-Luqueño**,[2] **and Javier Rodríguez-Varela**[2]

[1]*Conacyt-Cinvestav-IPN Unidad Saltillo, Sustentabilidad de Los Recursos Naturales y Energía, Ramos Arizpe, Coahuila C.P. 25900, Mexico*
[2]*Sustentabilidad de Los Recursos Naturales y Energía, Cinvestav Unidad Saltillo, Av. Industria Metalúrgica, 1062, C.P. 25900, Ramos Arizpe, Coah, Mexico*
[3]*Universidad Autónoma de NL, Facultad de Ingeniería Civil, San Nicolás de Los Garza, Nuevo León 66455, Mexico*
[4]*Conacyt, Centro de Investigación Científica de Yucatán, Col. Chuburná de Hidalgo, Calle 43, No. 130, Mérida, Yucatán C.P. 97200, Mexico*
[5]*Rathinam Research Center, Rathinam Technical Campus, Rathinam Techzone, Pollachi Main Road, Eachanari, Coimbatore – 641021, Tamilnadu, India*

Correspondence should be addressed to Ivonne L. Alonso-Lemus; ivalemus@gmail.com

Received 4 May 2022; Accepted 7 July 2022; Published 28 August 2022

Academic Editor: Dr Abhilash

In this work, electroactive biofilms of *Bacillus subtilis* (*B. subtilis*) or *Escherichia coli* (E. *coli*) were supported on functionalized biocarbon (AB7-F), which was synthesized from waste leather and was used as catalysts to develop bioanodes for microbial fuel cells (MFCs). This way, bioanodes were fabricated and further evaluated in a three-electrode cell using pharmaceutical wastewater (PWW) as substrate. The electrochemical measurements showed a higher performance of the bioanode based on AB7-f+ *B. subtilis* to oxidize organic matter from PWW. The polarization curves in the dual-chamber MFC showed that AB7-f+ *B. subtilis* bioanode can generate an open circuit voltage of 602 mV and a power density of 77 mW m^{-2}. During long-term tests of the MFC, a variation in performance was observed, with a maximum of 96.3 mW m^{-2} on day 7. Such variation was attributed to the development of more stable biofilm as well as consumption of some compounds metabolized by bacteria grown on the bioanode. The results showed that AB7-f+ *B. subtilis* can be used as bioanode for MFCs with PWW as substrate removing around 45% of the chemical oxygen demand (COD).

1. Introduction

Water pollution has emerged as a life-threating global problem due to rapid growth of urbanization, industrialization, and irrational utilization of water resources. All the effluents from different types of industries like fertilizers, textiles, diary processing, petrochemical, beverages, and pharmaceutical have toxicated the water to such an extent that all lives on this planet are affected. In this respect, industrial wastewater treatment is a big challenge issue. It is believed that nearly 80–90% of all industrial wastewater in developing countries is discharged untreated, causing severe environmental damage [1]. Among the various types of effluents, the one from the pharmaceutical must be treated with utmost vigilance due to the presence of organic pollutants and drug components [2]. In addition, the presence of pharmaceuticals in wastewater does not only come from industrial effluents, it is also found in domestic wastewater

[3]. Even though there are various methods for the treatment of pharmaceutical wastewater (PWW), which can be classified as physical, physicochemical, chemical, and biological methods, but all are accompanied with various challenges with low efficiency or economic infeasibility [4]. On the other hand, PWW treatment and simultaneously generating energy from it will support the waste management system, alongside sustainable means of energy generation. A vast number of research is going on bioelectrochemical systems (BES) [5]. Microbial fuel cell (MFC) has attained considerable remark due to the advantage of cost-effectiveness, high-biodegradability, and eco-friendly.

The MFCs transform the chemical energy into electrical energy by electrochemical active microorganism, known as exoelectrogens. In the anode chamber, organic matter is oxidized, producing electrons and protons. Electrons are transferred to the cathode chamber through an external circuit, where they react with oxygen and protons to form water [6]. Since electroactive bacteria can remove organic matter while generating electrical energy simultaneously, researchers focus the MFC as an alternative electrochemical technology for wastewater treatment and a sustainable energy resource. Despite this, MFCs' actual deployment has been hampered by their limited power output and expensive fabrication costs [7]. Recent research proves that modification in anaerobic anode chamber (e.g., active microorganism, bioanode configuration, and use of carbon-based catalysts) improve the total output power and performance. Since, the wastewater substrate is present in the anode chamber, the bioanode must be extremely active and electrochemically stable in wide range of pH. In this regard, a comprehensive variety of carbon material-based bioanodes has been evaluated for MFC applications [8, 9]. Biomass-derived biocarbons are rich in carbon with self-doped heteroatom, inexpensive, and eco-friendly with interesting surface chemistry and structural advantage over other precious metal material that have been used as catalysts in this application. Biocarbons from bamboo, cotton textiles, bananas, neem wood, silk cocoon, egg, and bread have been successfully demonstrated in bioanodes for MFC [8].

On the other hand, the growing interest in the development of high-efficient BES has led to the study of various exoelectrogenic cultures [9]. For example, anaerobic bacteria such as *Rhodoferax ferrireducens* and *Geobacter sulfurreducens* are studied as active microorganisms for MFC applications. When they meet exocellular solid substrates, they use outer membrane redox proteins (e.g., cytochromes) to mediate electron transfer [10]. Moreover, other bacteria like *Pseudomonas aeruginosa* and *Shewanella putrefaciens* create redox molecules as phenazine and quinones as electron carriers [11]. On the other hand, *Escherichia coli* (E. *coli*) create artificial redox molecules for extracellular electron transfer to solid substrates, and *Bacillus subtilis* (B. *subtilis*) has the advantage to be electrochemically active towards oxidation on wide range of pH in addition to being resistant to the presence of several antibiotics [12].

In our research group we have carried out previous studies for the treatment of PWW using *B. subtilis* growing on carbon-based catalyst, which improves the overall performance of MFC in terms of electricity generation and COD removal. In this concern, Duarte-Urbina et al. [12] reported decrease in chemical and biological oxygen demand (COD & BOD), total dissolved solids (TDS), and pH from 9.2–8.7 in PWW for 14 days of treatment in a dual-chamber MFC. In that work, bioanode is composed of onion waste-derived biocarbon+ *B. subtilis* showing a maximum power density (Pcell) of $30.72\,\mathrm{mW\,m^{-2}}$. Meanwhile, García–Mayagoitia et al. [13] reported stable bioanodes composed of functionalized ordered mesoporous carbon (f-OMC) + *B. subtilis* using PWW as a substrate (pH = 9.6). With this bioanode configuration, an open circuit voltage up to 0.62 V is obtained, with maximum current density and power density (Pcell) of $854\,\mathrm{mA\,m^{-2}}$ and $105\,\mathrm{mW\,m^{-2}}$, respectively.

In this work, we report the performance of dual-chambered H-type MFC, using a novel bioanode made with functionalized waste leather-derived biocarbon (AB7-F) plus *E. coli* and *B. subtilis* used separately as electrochemically active microorganisms and PWW as organic substrate. Whilst in the cathode chamber, a commercial Pt-based catalyst electrode and electrolyte of O_2-satured aqueous KOH solution (pH = 9.7) were used. An alkalinized Nafion membrane was used as a separator between anode and cathode chambers.

2. Experimental

2.1. Biocarbon Synthesis (Catalyst). The biocarbon was obtained based on a previous methodology reported by Alonso–Lemus et al. [14]. First, 10 g of leather waste slices were cleaned with ethanol (C_2H_5OH, Jalmek, 96%), then they were pyrolyzed at 700°C for 90 minutes at a heat rate of $10^{\circ}\mathrm{C\,min^{-1}}$ in N_2 atmosphere (Infra, 99.99%). The carbonized slices were pulverized and mixed with potassium hydroxide (KOH, Fermont, 87.5%) in a weight ratio of 2 : 1. Afterwards, this mixture was activated at 750°C for 90 minutes, at a heat rate of $8^{\circ}\mathrm{C\,min^{-1}}$ in N_2 atmosphere and cooled down to room temperature. Then, a black powder was recovered to wash it with an aqueous solution of $1\,\mathrm{mol\,L^{-1}}$ of hydrochloric acid (HCl, Sigma Aldrich, 37%) and dried overnight at 80°C. The biocarbon obtained was labeled as AB7.

AB7 was functionalized by intermittent microwave heating (IMH) to improve its biocompatibility [13] as follows: 300 mg of AB7 were dispersed in 30 mL of $0.15\,\mathrm{mol\,L^{-1}}$ methanol (CH_3OH, Sigma Aldrich, 99.8%) aqueous solution by sonication for 30 minutes. Then, the dispersion was stirred for one hour more and transferred to a modified homemade microwave maintaining magnetic stirring. The thermal treatment by IMH was for 8 minutes with 25 s on/15 s off pulses. The functionalized biocarbon was labeled as AB7-f.

2.2. Bioanodes Construction. As shown in Figure 1, the bioanodes were composed of three layers: support, catalytic layer, and biofilm. Carbon cloth was used as a support with a geometric area of $2\,\mathrm{cm^2}$ (1×2 cm). A copper wire was fixed

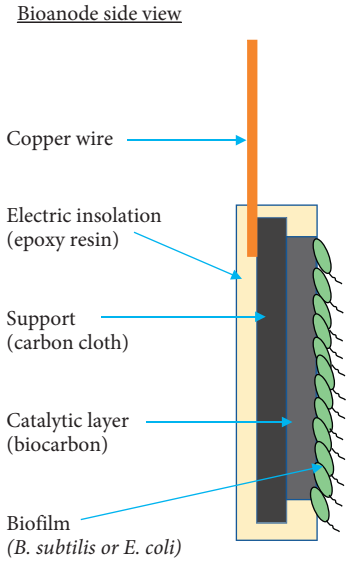

Figure 1: Bioanode side view with a configuration of support + catalysts + biofilm.

on its back using silver ink, then an area of 1 cm^2 of the carbon cloth was delimited with epoxy resin. Afterwards, the catalytic layer was deposited on the delimited area by drop-by-drop method (catalyst loading = 5 mg cm^{-2}). The catalytic ink had the following composition: 5 mg of catalyst, 64 μL of Nafion® 117 solution (Aldrich 5 wt. %), and 64 μL of 2-propanol (C_3H_7OH, Sigma Aldrich, 99.5%). The anodes (support + catalytic layer) were stored in a desiccator until to use them.

For the biofilm layer two bacteria were used separately: *Bacillus subtilis* (*B. subtilis*), which was obtained from the Cinvestav National Collection of Microbial Strains and Cell Cultures, whilst *Escherichia coli* (*E. coli*) ATCC® 25922™ was supplied by Microbiologics®. Inoculation of the strains from their reception until their use for the growth of the biofilm can be consulted in supplementary information. For the biofilm grown on the anodes, first, bacteria were inoculated at 30°C for 3 days using an orbital incubator (Vichi, INC-C); then the anodes were immersed into 50 mL of sterile broth media contained in an Erlenmeyer flask and inoculated for 6 days at 30°C in the orbital incubator (Figure S1(a)).

2.3. Pharmaceutical Wastewater (PWW) Substrate. The PWW was provided by a local pharmaceutical industry. The PWW was collected and stored at -18°C to preserve it until its use. The physicochemical features of the PWW are shown in Table 1.

2.4. Physicochemical Characterization. Morphology and elemental composition of the bioanodes were determined using a scanning electron microscope (SEM) Philips XL 30 ESEM with an EDAX detector. Moreover, the structural features of the catalysts were analyzed using a DXR-RAMAN thermo scientific spectrometer (He–Ne laser of 633 nm, 0.3 mW). Meanwhile, their functional groups were determined using a Bruker Tensor II equipment with ATR, in a range of 4000 to 500 cm^{-1} with a resolution of 4 cm^{-1}. In addition, an ASAP 2050 equipment (Micrometrics, USA) was used to determine the textural properties of the catalysts. Prior to the measurements, the samples were degassed for 14 h at 220°C, then nitrogen was used as absorbate.

Table 1: Physicochemical parameters of the PWW used as substrate.

Parameter	Value
pH	9.2
Conductivity	2870 mS m^{-1}
Chemical oxygen demand (COD)	27,603 mg L^{-1}
Biochemical oxygen demand (BOD)	10,433 mg L^{-1}
Nitrate nitrogen ($N–NO_3$)	6.13 mg L^{-1}
Total phosphorus	93.91 mg L^{-1}
Sulfate ion (SO^{2-}_4)	1,161 mg L^{-1}
Total alkalinity	3,574 mg L^{-1} $CaCO_3$
Chloride	10,616 mg L^{-1}
Total dissolved solids (TDS)	30,540 mg L^{-1}
Total suspended solids (TSS)	3,320 mg L^{-1}

2.5. Electrochemical Measurements

2.5.1. Half-Cell. The electrochemical measurements were performed using a Bio-Logic VSP-300 potentiostat in a three-electrode cell configuration. A platinum wire and a Ag/AgCl (NaCl 3 mol L^{-1}, 0.209 V vs. SHE) were used as counter and reference electrodes, respectively. The work electrodes (WE) were the anodes (support + catalyst) and bioanodes (support + catalyst + bacteria) previously made. Prior to the electrochemical test, the WE were stabilized for 18 hours into the N_2-saturated PW at room temperature, which was used as substrate. The Cyclic Voltammetry (CV) curves were obtained in a potential range of -0.70 to 0.45 V vs. the reversible hydrogen electrode (RHE) at a scan rate of 20 mV s^{-1}. For comparison purposes, CVs of the support and support + bacteria were obtained.

All the potential reported in this work were converted to the RHE voltage (E_{RHE}) using the following equation [15]:

$$E_{RHE} = E + 0.059\,pH + E_{\text{ref}}, \quad (1)$$

where the pH of the PWW is 9.2, E_{ref} is the potential of the reference electrode versus the standard hydrogen electrode (SHE), and E in the potential that is wanted to convert to E_{RHE}.

2.5.2. Microbial Fuel Cell Test. The most active bioanode was tested in a dual-chambered H-type MFC (Figure S1(b)). The anode chamber contained 240 mL of N_2-satured PW and the bioanode previously stabilized for 18 hours. Whilst in the cathode chamber a commercial Pt-based catalyst electrode (Etek, 20 wt. % Pt/C, catalyst load = 2 mg cm^{-2}) and electrolyte of O_2-satured aqueous KOH solution (pH = 9.7) were used. A Nafion® 117 (DuPont) membrane was used as separator, which was previously alkalinized as was described in supplementary information [16]. First, the open circuit

potential (E_{OC}) was determined, then, the cell potential (E_{cell}) was registered at different external resistance values (R_{ext} = 0.01, 1, 1.2, 5, and 10 kΩ). The cell current (I_{cell}) was calculated by the Ohm's law (2)

$$I_{cell} = \frac{E_{cell}}{R_{ext}}. \quad (2)$$

Then, the current density (j_{cell}) was calculated normalizing the I_{cell} respect to the geometrical bioanode area (A_{bio}). Thus, the polarization curve (E_{cell} vs. j_{cell}) plots were obtained. Finally, the power density (P_{cell}) was calculated as follows (3):

$$P_{cell} = \frac{E_{cell}^2}{R_{ext} \cdot A_{bio}}. \quad (3)$$

Both, the polarization (E_{cell} vs. j_{cell}) and power density (P_{cell} vs. j_{cell}) plots were obtained at day 0, 1, 7, and 14.

3. Results and Discussion

3.1. Catalysts Physicochemical Properties. Figure 2(a) shows the chemical composition of the catalysts and the raw material used for their synthesis (leather), which was determined by energy-dispersive X-ray spectroscopy (EDS). As can be seen, leather was composed mainly of carbon (69.62 wt. %) and oxygen (18.89 wt. %), in addition to some heteroatoms like nitrogen (4.13 wt. %) and sulfur (3.10 wt. %). Also, other elements in less concentration were detected (e.g., Ca, Na, Mg, and Si). As it was expected, the carbon concentration of both AB7 and AB7-f catalysts increased ($C \sim 89$ wt. %) and the oxygen decreased ($O \sim 7$ wt. %) respect to leather due to pyrolysis treatment. Further, it was observed that the remaining concentration of nitrogen ($N \sim 2$ wt. %) and sulfur ($S \sim 0.1$ wt. %) was lower for both catalysts than leather, which implies that by the synthesis route proposed in this work, heteroatom self-doped catalysts could be obtained. On the other hand, it was observed that elements contained in leather in low concentration were removed from both AB7 and AB7-f, where only Mg was detected in concentrations of 0.17 and 0.14 wt. %, respectively. The chemical composition values also can be found in Table S2*; meanwhile, Figure S2* shows the elemental mapping of the catalysts which demonstrate that both catalysts had a homogeneous distribution of the elements.

Figure 2(b) shows the typical morphology of leather's collagen fibers about a micron in diameter. Interestingly, the morphology of the collagen fibers was lost after the carbonization and activation treatment to which AB7 was subjected, as shown in Figure 2(c). As can be seen, collagen fibers sinterized until forming 3D particles interconnected by macropores. However, AB7-f revealed carbon particles of smaller size than the AB7 particles, which indicates that microwave heating could promote the reduction in particle size, as has been reported [12, 13].

On the other hand, the catalysis' structural and textural features were studied (Figure 3). Raman spectroscopy of AB7 and AB7-f are shown in Figures 3(a) and 3(b), respectively. Two broad bands normally observed in amorphous carbon materials were detected, the first one at ≈1330 cm^{-1}, named D-band, which can be associated to defects and disorder in the graphitic lattice. The second signal at ≈1600 cm^{-1}, named G-band, is normally associated with sp^2 hybridization. The I_D/I_G ratio was calculated from the deconvoluted peaks showing little variation between the values found for AB7 (I_D/I_G = 1.58) and AB7-f (I_D/I_G = 1.50). However, when the ratio between D2 interband (≈1200 cm^{-1}) and G band was calculated, a difference was observed between AB7 (I_{D2}/I_G = 1.12) and AB7-f (I_{D2}/I_G = 0.46). The D2 interband, also called D^* has been attributed sp^2-sp^3 bond in carbon lattice [17], and when its value decreases it can be assumed that the crystallinity in the nanodomains increases, therefore, AB7-f has a more crystalline nanodomain structure than AB7. This occurs because microwave heating promotes the release of carbon and oxygen from the carbon material, generating small conjugated graphitic domains, which improves crystallinity [18]. In addition, D3 interband (≈1500 cm^{-1}) can be related to small functional groups and SP2-bonded forms, and it has been reported that when D3 interband intensity decrease the crystallinity increase [19], which is in good agreement with our results.

Figure 3(c) shows the nitrogen adsorption/desorption isotherms of the catalyst. According to the international union of pure and applied chemistry (IUPAC) classification [20], the adsorption isotherms of both AB7 and AB7-f are type IV(a), which are commonly observed for mesoporous materials with pores greater than 4 nm. In addition, both isotherms show a hysteresis loop H4 type, indicating the filling of micropores. Therefore, it can be assumed that AB7 and AB7-f are micro-mesoporous carbon materials [21]. The specific surface area was calculated by Brunauer–Emmett–Teller method (SSA_{BET}). As it was expected, high surface area values were obtained for AB7 (SSA_{BET} = 1890 m^2g^{-1}) and AB7-f (SSA_{BET} = 1984 m^2g^{-1}) because KOH was used as a chemical activating agent and it mainly promotes the formation of micropores generating high surface area carbons. Moreover, the average pore size of AB7 and AB7-f was of 4.4 nm and 5.5 nm, respectively. The slight increase of 4% in SSA_{BET} of AB7-f with respect to AB7, and the increase in the average pore size is because, as already mentioned, during microwave heating, carbon and oxygen were expelled, generating the formation of additional pores and the increase in the average pore size. On the other hand, Figure 3(d) shows the Fourier–transform infrared (FTIR) spectra of the catalysts. As can be seen, there are two broad peaks in the range of 1400–1600 cm^{-1} and 1650–1900 cm^{-1}. In the first region, the signal associated to the combined stretching of *C*=*C* and C–C of aromatic compounds was observed. Meanwhile, in the second region, the corresponding *C*=*O* bond can be found. The presence of C–H bond at ≈ 2600 cm^{-1} generated by aldehyde type bond also was detected [22, 23].

3.2. Bioanodes Morphology and Performance in Half-Cell. Figure 4 shows the morphology of bioanodes with different configurations. The micrographs in Figures 4(a) and 2(b)

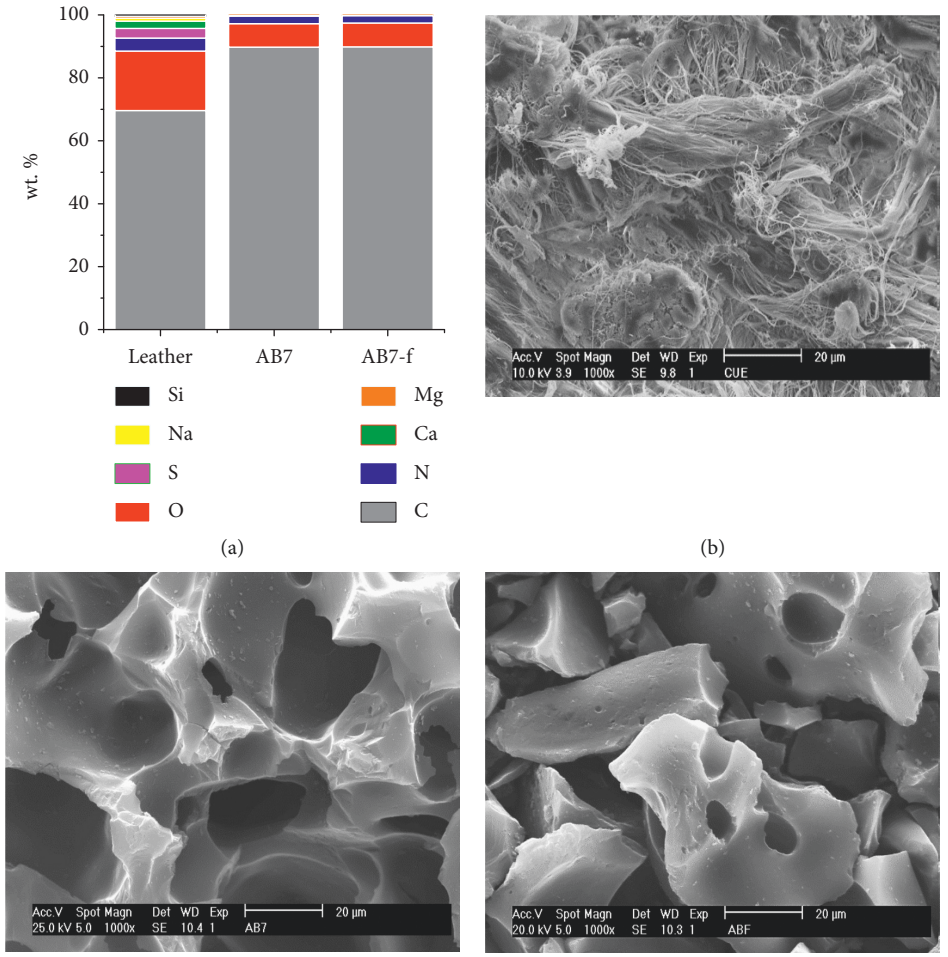

Figure 2: (a) Chemical composition of leather and catalysts determined by EDS and morphology of (b) leather, (c) AB7, and (d) AB7-f.

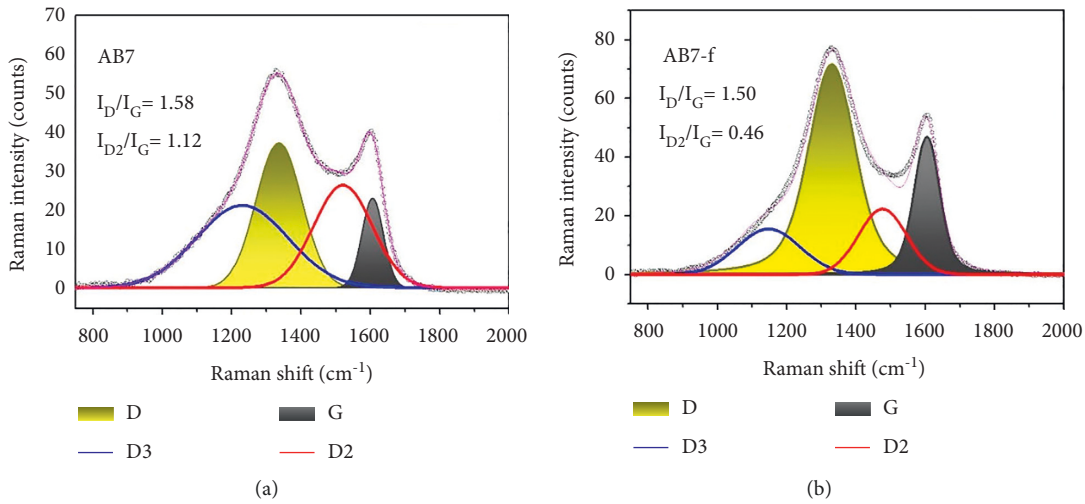

Figure 3: Continued.

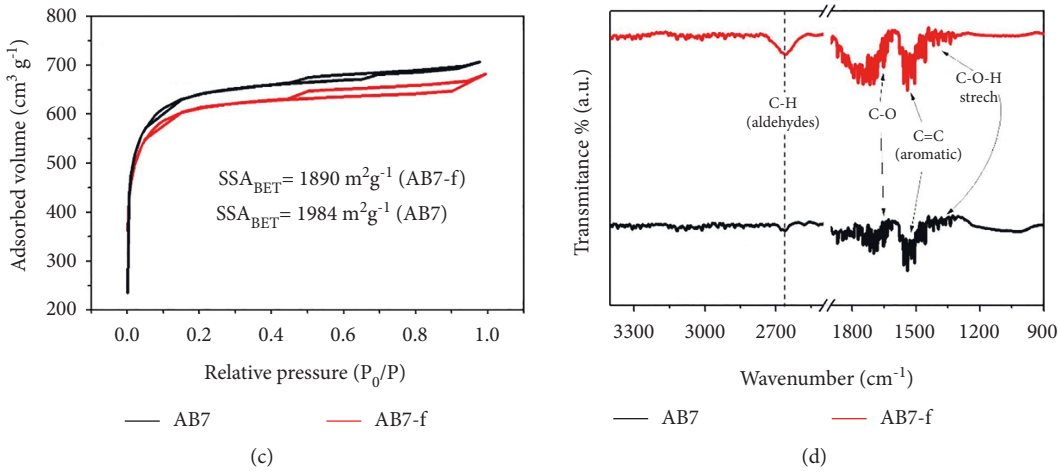

FIGURE 3: Structural and textural features of the catalysts. Raman spectroscopy of (a) AB7 and (b) AB7-f, (c) adsorption/desorption isotherms, and (d) Fourier-transform infrared spectra of the catalysts.

show the bioanodes with *S* + AB7 + *E. coli* and *S* + AB7-f + *E. coli* configurations, respectively. As can be seen, groups of bacteria are observed on the surface of the catalysts with a quasi-spherical shape, which may indicate that they are in an early stage of development, since the characteristic morphology of *E. coli* is that of bacilli (smaller than those of *B. subtilis*). Despite the presence of these bacteria, an inhomogeneous growth of biofilm on the surface of the catalytic layer has been observed. However, for the bioanode with the *S* + AB7-f + *E. coli* configuration, a greater growth of the bacteria is observed compared to the non-functionalized catalyst (Figure 4(b)). Meanwhile, the bioanode with *S* + AB7 + *B. subtilis* configuration (Figure 4(c)) shows the presence of some isolated bacilli on a smooth surface. That change in surface texture can be attributed to polysaccharides excreted during biofilm formation [24]. Figure 4(d) shows the bioanode with *S* + AB7-f + *B. subtilis* configuration. It should be noted the outstanding biocompatibility of the bioanode, the growth of the *B. subtilis* biofilm on this catalyst is abundant, forming a reticular structure that almost completely covers the surface of the catalyst. Interestingly, these results indicate that functionalized catalysts improve biocompatibility, which is in good agreement with observations from our previous studies [12, 13].

The electrochemical performance of all bioanodes was evaluated in half-cell system. First, the cyclic voltammetry (CV) curves of support (S) + bacteria using N_2-saturated PWW as substrate were obtained (Figure 5(a)). In general, the electrochemical behavior of the supports with and without biofilm is very similar. The sweep in the cathodic direction had shown an increase in the current density (j) near to 0.45 V/RHE, which is more notable for *S* + *B. subtilis*. These results confirm the need to use a catalyst to promote the generation of redox couples.

In Figure 5(b) the CV of the bioanode *S* + AB7 has shown a similar shape to those CVs of Figure 5(a), although with highest values of j in the same potential range, this increase in j can be attributed to the effect of the catalyst AB7, which increases the electrode-electrolyte interaction due to its high surface area [25]. Whilst for *S* + AB7 + *B. subtilis* bioanode j decreases suggesting low electroactivity. Furthermore, the VC of the *S* + AB7 + *E. coli* bioanode shows a quasi-capacitive behavior indicating a better bioelectrochemical interaction with organic matter of PWW than the previous two bioanodes.

In Figure 5(c), the VC of the anode *S* + AB7-f also shows a quasicapacitive behavior, which suggests catalytic activity of AB7-f in PWW. Remarkably, the bioanode *S* + AB7-f + *B. subtilis* generates the highest values of j, with a capacitive behavior. This indicates a high catalytic activity of this bioanode to oxidize the organic matter in the PWW. In addition, this result suggests a positive effect of the functionalization treatment by modifying the surface of the catalyst, and thus, improving the biocompatibility. In contrast, the VC of the bioanode *S* + AB7-f + *E. coli* has lower *j* values than *S* + AB7-f + *B. subtilis*, due mainly to the low biocompatibility between AB7-f and *E. coli,* which implies a low electroactivity to oxidize PWW organic matter. In the case of this study, the electrochemical behaviors observed in Figure 5 can be attributed to the nature of both catalysts (chemical composition, morphology, specific area, structure, and texture) since it has been reported that there is not a direct relationship between the amount of biofilm and the current density generated [26]. It has also been reported that the presence of oxygenated groups in the catalysts where the biofilm grows can increase the catalyst-bacteria biocompatibility [27, 28].

3.3. Bioanodes Morphology and Performance in Half-Cell. With the results obtained from the electrochemical characterization in half-cell, it was decided to use the bioanode *S* + AB7-f + *B. subtilis* for the electrochemical characterization and PWW remediation tests in a dual-chamber MFC. Figure 6(a) shows the E_{cell}-j polarization curve (black triangle) and the P_{cell}-j curve (red square) obtained at the

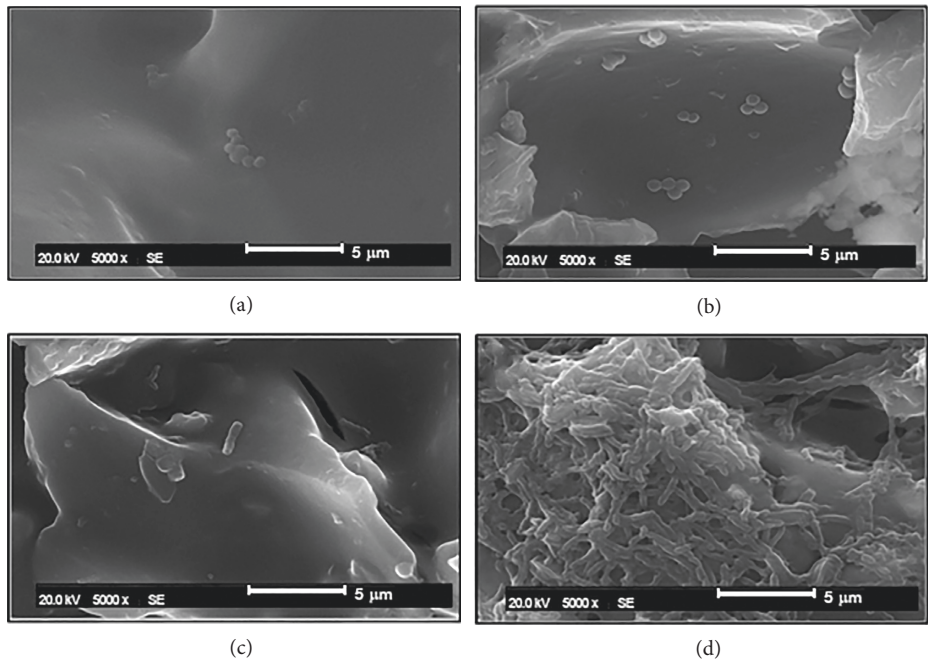

Figure 4: Bioanodes morphology with different configurations. (a) *S* + AB7 + *E. coli*, (b) *S* + AB7-f + *E. coli*, (c) *S* + AB7 + *B. subtilis*, and (d) *S* + AB7-f + *B. subtilis*.

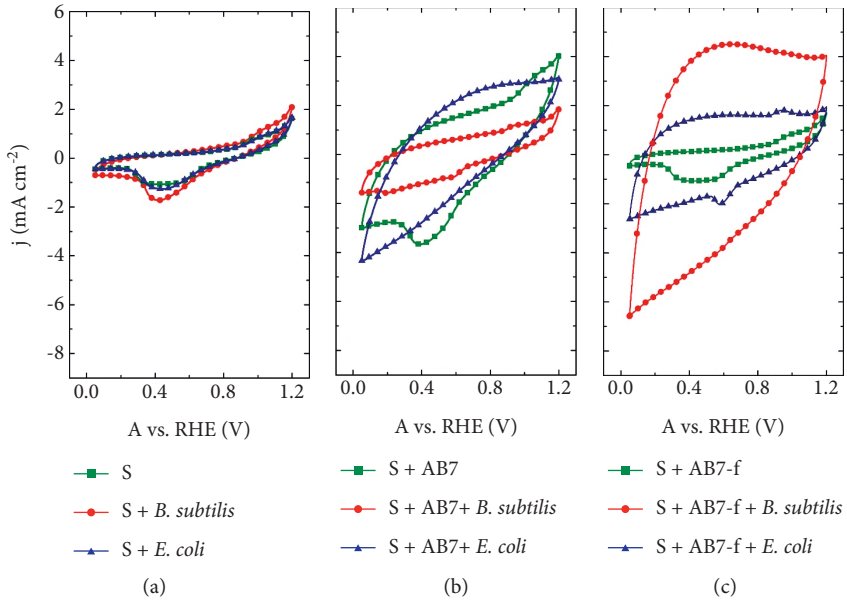

Figure 5: Half-cell characterization of the bioanodes with different configurations using N_2-saturated PWW as substrate at a scan rate of 20 mV s^{-1} and as support (S) carbon cloth, (a) *S* + bacteria, (b) *S* + AB7 + bacteria, and (c) *S* + AB7-f + bacteria.

beginning of the long-term test. The initial E_{cell} was of 0.60 V, with a maximum value of $P_{cell} = 77$ mW m^{-2} and $j = 254$ mA m^{-2}. The linear tendence of the E_{cell}-j polarization curve indicates a good mass transport to the electrode, which suggests that the bioanode *S* + AB7-f + *B. subtilis* biofilm reduces the diffusional and electrochemical limitations [29]. In addition, no significant voltage drops were observed at the beginning of the test, which implies that activation losses to carry out the redox reaction was low [30, 31], maybe due to synergic interaction of several characteristics of the bioanodes such as high specific surface area of the catalysts (AB7-f), good biocompatibility between AB7-f and *B. subtilis* and good performance in PWW substrate [30]. Figure 6(b) shows P_{cell}-j curves obtained during the long-term test (initial, day 1, 7, and 14). As can be seen, the P_{cell} generates by the MFC varies over time. The better

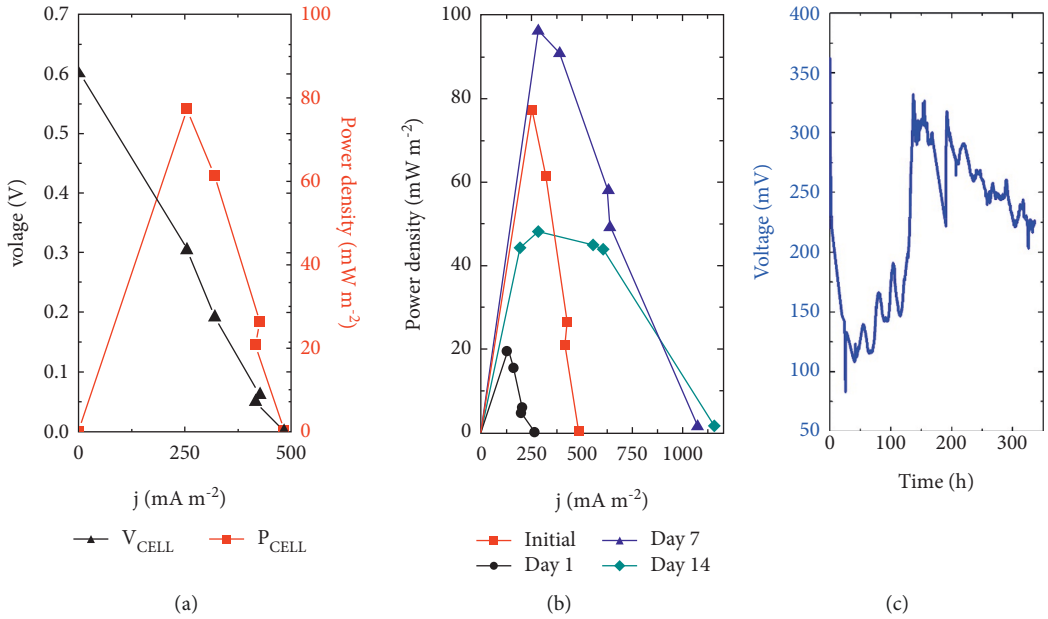

Figure 6: Long-term test of the MFC. Anode chamber: *S* + AB7-f + *B. subtilis* bioanode and PWW as substrate (pH = 9.2). Cathode chamber: 20% Pt/C catalysts in KOH (pH = 9.7) electrolyte. Nafion® 117 alkalinized membrane was used as separator. (a) E_{cell}-j and P_{cell}-j curves obtained at the initial of the test, (b) P_{cell}-j curves obtained during the initial, days 1, 7, and 14, and (c) open circuit voltage of the MFC vs. time using a R_{ext} = 10 kΩ.

Table 2: Electrochemical parameters of the MFC during the long-term test.

Time	E_{cell} (V)	Maximum P_{cell} (mW m^{-2})	j (mA m^{-2})	Pv (mW m^{-3})
Initial	0.60	77.4	254	38.7
Day 1	0.31	19.3	127	9.6
Day 7	0.53	96.3	283	48.1
Day 14	0.38	48.1	283	24.0

performance was observed on day 7 with a maximum of P_{cell} = 96.3 mW m^{-2}. Meanwhile, the oscillating P_{cell} generation in the MFC is because it is a dynamic system, where the biofilm of *B. subtilis* could be modified in the presence of PWW (formation/shedding of other bacteria) [32].

Table 2 summarized the electrochemical parameters obtained from Pcell-j curves at different times. The Ecell values at initial and day 7 were similar (≈0.6 V) and is consistent with previously reported MFC voltages with similar arrays (Ecell between 0.5 and 0.8 V) [33]. Therefore, it can be assumed that in these periods of time, the system was in optimal conditions.

On the other hand, the maximum P_{cell} values obtained in this work are comparable with other previously reported (Table S3). In this work, we used PWW (as received from the industry) and *S* + AB7-f + *B. subtilis* as bioanode, meanwhile, other reports operating the MFC with more controllable parameters (e.g., synthetic substrates and mixed cultures). However, the comparison between different types of MFC systems is complicated, since there are many variables, such as the substrate, electrodes, use of catalysts, cell configuration, temperature, pH, and bacteria [34]. Therefore, with this comparison we want to highlight that *S* + AB7-f + *B. subtilis* bioanode is promising to generate bioenergy even in recalcitrant media as the PWW.

Figure 6(c) shows the E_{cell}-time curve applying a R_{ext} of 10 kΩ to the MFC during the 14 days of testing. Under this condition, the initial $E_{cell(10\ k\Omega)}$ was of 360 mV, which continuously decreases until 83 mV, the lowest $E_{cell(10\ k\Omega)}$ value recorded at 25 h. This voltage drop may be caused by the processes of stabilization and adaptation in the bioelectrochemical system. In a period from 25 to 130 hours, a constant increase in voltage was observed until reaching voltages above 300 mV; where interestingly it can be seen that there are periods where the voltage slightly decreases, which coincides with the night periods. After 130 h, the voltage is relatively constant until 160 h, then, the voltage decreases to 224 mV. These results confirm that the best performance is between 130 and 168 h (5–7 days). Meanwhile, the voltage decreases towards the end of the long-term test may be due to decrease in nutrients assimilable by the bacteria near to the bioanode [35]. It is important to note that this is a batch process without agitation, so the diffusion of nutrients to the bioanode may be limited. This behavior has also been reported for MFC with complex organic matter such as aromatic compounds [36], paper recycling [37], and wastewater from the coke production process [38].

Finally, Table 3 shows the physicochemical parameters of PWW during the long-term test. As can be seen, there was a

Table 3: Physicochemical parameters of PWW at different times during the long-term test. No determined.

Parameter	Units	Long-term test			
		Initial (0 h)	Day 1 (24 h)	Day 7 (168 h)	Day 14 (336 h)
pH		9.20	9.10	8.60	8.50
Conductivity	mS m^{-1}	2,870	2,830	2,810	2,770
Chemical oxygen demand (COD)	mg L^{-1}	27,603	22,694	21,384	15,181
Biochemical oxygen demand (BOD)	mg L^{-1}	10,433	—	—	8,900
Nitrates (N–NO_3)	mg L^{-1}	6.13	—	—	6.76
Total phosphorous	mg L^{-1}	93.91	—	—	91.15
Sulfate ion (SO^{2-}_4)	mg L^{-1}	1,161	—	—	3,592
Alkalinity	mg L^{-1} $CaCO_3$	3,574	—	—	3,772
Chlorides	mg L^{-1}	10,616	—	—	9,466
Total dissolved solids (TDS)	mg L^{-1}	30,540	—	—	27,900
Total suspended solids (TSS)	mg L^{-1}	3,320	—	—	1,640

gradual decrease in pH from 9.2 to 8.5, while the electrical conductivity remains relatively constant. Regarding the chemical and biochemical oxygen demand, the removal of these in this work was of 45 and 15% of COD and BOD, respectively. The sulfates ion (SO^{-4}) increases almost three times on day 14 compared to its initial value. Meanwhile, total dissolved and suspended solids decrease 8.5 and 50.6%, respectively. Other chemical parameters such as nitrates, phosphorous, and alkalinity remains constant.

4. Conclusions

4.1. The most important findings of this work are the following. Amorphous carbon-based catalysts were successfully obtained from waste leather labeled as AB7 and AB7-f, both with a carbon content greater than 90% and high S_{BET} (up to 1984 $m^2 g^{-1}$). Furthermore, the results prove that subjecting the catalysts to a microwave intermittent heating (MIH) treatment improves the biocompatibility between it and the bacteria.

The bioanode *S* + AB7-f + *B. subtilis* has an outstanding performance in half-cell and MFC systems for the generation of energy and remediation of PWW. The maximum P_{cell} of 96.3 mW m^{-2} was observed on day 7, achieving a removal of up to 45% of COD on day 14. Therefore, the development of catalysts made from leather waste in conjunction with PWW as a substrate and *B. subtilis* as an electroactive microorganism for use in MFCs is considered promising [39, 40].

Data Availability

No databases are included in this study.

Conflicts of Interest

The authors declare that they have no conflicts of interest.

Acknowledgments

The authors want to thank the Mexican National Council of Science and Technology for the financial support through grants 250632 and 241526. J. M. Baas-López is acknowledged for his valuable support with the physicochemical characterization (XRD, FTIR, and Raman spectra).

Supplementary Materials

Figure S1. (a) Biofilm grow method and (b) dual-chambered H-Type MFC configuration used in this work. Table S2. Chemical composition of leather and leather-derived catalysts determined by EDS technique. Figure S2. Elemental mapping of the leather waste-derived catalyst AB7 and AB7-f. Table S3. Reports of different MFC configurations and the maximum power density compared with this work. (*Supplementary Materials*)

References

[1] V. V. Ranade and V. M. Bhandari, "Chapter 1: industrial wastewater treatment, recycling and reuse: an overview," in *Industrial Wastewater Treatment, Recycling and Reuse*, pp. 1–80, Butterworth-Heinemann. Copyright © 2014 Elsevier Ltd. All rights reserved, Amsterdam, Netherlands, 2014.

[2] K. Aguilar-Pérez, J. Aviles-Castillo, and G. Ruiz-Pulido, "Nano-sorbent materials for pharmaceutical-based wastewater effluents-An overview," *CSCEE*, vol. 2, Article ID 100028, 2020.

[3] D. Cecconet, D. Molognoni, A. Callegari, and A. G. Capodaglio, "Biological combination processes for efficient removal of pharmaceutically active compounds from wastewater: a review and future perspectives," *Journal of Environmental Chemical Engineering*, vol. 5, no. 4, pp. 3590–3603, 2017.

[4] G. Crini and E. Lichtfouse, "Advantages and disadvantages of techniques used for wastewater treatment," *Environmental Chemistry Letters*, vol. 17, no. 1, pp. 145–155, 2019.

[5] M. M. Ghangrekar, S. Das, and B. R. Tiwari, "11 - integration of bioelectrochemical systems with other existing wastewater treatment processes," in *Integrated Microbial Fuel Cells for Wastewater Treatment*Copyright © 2020 Elsevier Inc. All rights reserved, Amsterdam, Netherlands, 2020.

[6] T. Rashid, F. Sher, A. Hazafa et al., "Design and feasibility study of novel paraboloid graphite based microbial fuel cell for bioelectrogenesis and pharmaceutical wastewater treatment," *Journal of Environmental Chemical Engineering*, vol. 9, no. 1, Article ID 104502, 2021.

[7] M. E. Elshobary, H. M. Zabed, J. Yun, G. Zhang, and X. Qi, "Recent insights into microalgae-assisted microbial fuel cells for generating sustainable bioelectricity," *International Journal of Hydrogen Energy*, vol. 46, no. 4, pp. 3135–3159, 2021.

[8] X. Fan, Y. Zhou, X. Jin, R.-B. Song, Z. Li, and Q. Zhang, "Carbon material-based anodes in the microbial fuel cells," *Carbon Energy*, vol. 3, pp. 449–472, 2021.

[9] Y. Liu, X. Zhang, Q. Zhang, and C. Li, "Microbial fuel cells: nanomaterials based on anode and their application," *Energy Technology*, vol. 8, no. 9, Article ID 2000206, 2020.

[10] W. Yang and S. Chen, "Biomass-derived carbon for electrode fabrication in microbial fuel cells: a review," *Industrial & Engineering Chemistry Research*, vol. 59, no. 14, pp. 6391–6404, 2020.

[11] B. E. Logan, "Exoelectrogenic bacteria that power microbial fuel cells," *Nature Reviews Microbiology*, vol. 7, no. 5, pp. 375–381, 2009.

[12] T. Zhang, C. Cui, S. Chen, H. Yang, and P. Shen, "The direct electrocatalysis of *Escherichia coli* through electroactivated excretion in microbial fuel cell," *Electrochemistry Communications*, vol. 10, no. 2, pp. 293–297, 2008.

[13] F. Kracke, I. Vassilev, and J. O. Krömer, "Microbial electron transport and energy conservation - the foundation for optimizing bioelectrochemical systems," *Frontiers in Microbiology*, vol. 6, p. 575, 2015.

[14] O. J. Duarte-Urbina, F. J. Rodríguez-Varela, F. Fernández-Luqueño et al., "Bioanodes containing catalysts from onion waste and Bacillus subtilis for energy generation from pharmaceutical wastewater in a microbial fuel cell," *New Journal of Chemistry*, vol. 45, no. 28, pp. 12634–12646, 2021.

[15] S. García-Mayagoitia, F. Fernández-Luqueño, D. Morales-Acosta et al., "Energy generation from pharmaceutical residual water in microbial fuel cells using ordered mesoporous carbon and bacillus subtilis as bioanode," *ACS Sustainable Chemistry & Engineering*, vol. 7, no. 14, pp. 12179–12187, 2019.

[16] D. Lardizabal-Guitierrez, D. González-Quijano, P. Bartolo-Pérez, B. Escobar-Morales, F. J. Rodríguez-Varela, and I. L. Alonso-Lemus, "Communication—synthesis of self-doped metal-free electrocatalysts from waste leather with high ORR activity," *Journal of the Electrochemical Society*, vol. 163, no. 2, pp. H15–H17, 2015.

[17] G. Jerkiewicz, "Standard and reversible hydrogen electrodes: theory, design, operation, and applications," *ACS Catalysis*, vol. 10, no. 15, pp. 8409–8417, 2020.

[18] L. L de Souza, "Direct oxidation of ethylene glycol on PtSn/C for application in alkaline fuel cell," *International Journal of Electrochemical Science*, vol. 12, pp. 11855–11874, 2017.

[19] A. Sadezky, H. Muckenhuber, H. Grothe, R. Niessner, and U. Pöschl, "Raman microspectroscopy of soot and related carbonaceous materials: spectral analysis and structural information," *Carbon*, vol. 43, no. 8, pp. 1731–1742, 2005.

[20] P. Tang, G. Hu, Y. Gao et al., "The microwave adsorption behavior and microwave-assisted heteroatoms doping of graphene-based nano-carbon materials," *Scientific Reports*, vol. 4, no. 1, pp. 5901–5907, 2014.

[21] S. Vollebregt, R. Ishihara, F. D. Tichelaar, Y. Hou, and C. I. M. Beenakker, "Influence of the growth temperature on the first and second-order Raman band ratios and widths of carbon nanotubes and fibers," *Carbon*, vol. 50, no. 10, pp. 3542–3554, 2012.

[22] M. Thommes, K. Kaneko, A. V. Neimark et al., "Physisorption of gases, with special reference to the evaluation of surface area and pore size distribution (IUPAC Technical Report)," *Pure and Applied Chemistry*, vol. 87, no. 9-10, pp. 1051–1069, 2015.

[23] H. Marsh and F. Rodríguez-Reinoso, "Chapter 2 - activated carbon (origins)," in *Activated Carbon*, pp. 13–86, Elsevier Science, Oxford, U.K, 2006.

[24] R. Ali, Z. Aslam, R. A. Shawabkeh, A. Asghar, and I. A. Hussein, "BET, FTIR, and Raman characterizations of activated carbon from wasteoil fly ash," *Turkish Journal of Chemistry*, vol. 44, no. 2, pp. 279–295, 2020.

[25] S. Shin, J. Jang, S.-H. Yoon, and I. Mochida, "A study on the effect of heat treatment on functional groups of pitch based activated carbon fiber using FTIR," *Carbon*, vol. 35, no. 12, pp. 1739–1743, 1997.

[26] M. Schechter, A. Schechter, S. Rozenfeld, E. Efrat, and R. Cahan, "4. Anode biofilm," in *Technology and Application of Microbial Fuel Cells*InTech Open Access Books, London, U. K, 2014.

[27] S. H. Hassan, Y. S. Kim, and S. E. Oh, "Power generation from cellulose using mixed and pure cultures of cellulose-degrading bacteria in a microbial fuel cell," *Enzyme and Microbial Technology*, vol. 51, no. 5, pp. 269–273, 2012.

[28] S. A. Patil, F. Harnisch, B. Kapadnis, and U. Schroder, "Electroactive mixed culture biofilms in microbial bioelectrochemical systems: the role of temperature for biofilm formation and performance," *Biosensors and Bioelectronics*, vol. 26, no. 2, pp. 803–808, 2010.

[29] Y. Zhao, Y. Ma, T. Li, Z. Dong, and Y. Wang, "Modification of carbon felt anodes using double-oxidant HNO3/H2O2 for application in microbial fuel cells," *RSC Advances*, vol. 8, no. 4, pp. 2059–2064, 2018.

[30] X. Zhou, X. Chen, H. Li, J. Xiong, X. Li, and W. Li, "Surface oxygen-rich titanium as anode for high performance microbial fuel cell," *Electrochimica Acta*, vol. 209, pp. 582–590, 2016.

[31] V. R. Nimje, C.-Y. Chen, C.-C. Chen et al., "Stable and high energy generation by a strain of Bacillus subtilis in a microbial fuel cell," *Journal of Power Sources*, vol. 190, no. 2, pp. 258–263, 2009.

[32] B. E. Logan, B. Hamelers, R. Rozendal et al., "Microbial fuel cells: methodology and technology," *Environ. Sci. Technol.*vol. 40, no. 17, pp. 5181–5192, 2006.

[33] L. Peixoto, B. Min, G. Martins et al., "In situ microbial fuel cell-based biosensor for organic carbon," *Bioelectrochemistry*, vol. 81, no. 2, pp. 99–103, 2011.

[34] B. Min, J. Kim, S. Oh, J. M. Regan, and B. E. Logan, "Electricity generation from swine wastewater using microbial fuel cells," *Water Research*, vol. 39, no. 20, pp. 4961–4968, 2005.

[35] L. Peixoto, A. L. Rodrigues, G. Martins et al., "A flat microbial fuel cell for decentralized wastewater valorization: process performance and optimization potential," *Environmental Technology*, vol. 34, no. 13-14, pp. 1947–1956, 2013.

[36] S. Srikanth, M. Kumar, D. Singh, M. P. Singh, and B. P. Das, "Electro-biocatalytic treatment of petroleum refinery wastewater using microbial fuel cell (MFC) in continuous mode operation," *Bioresource Technology*, vol. 221, pp. 70–77, 2016.

[37] E. Herrero-Hernández, T. Smith, and R. Akid, "Electricity generation from wastewaters with starch as carbon source using a mediator less microbial fuel cell," *Biosensors and Bioelectronics*, vol. 39, no. 1, pp. 194–198, 2013.

[38] S. K. F. Marashi, H. R. Kariminia, and I. S. P. Savizi, "Bimodal electricity generation and aromatic compounds

removal from purified terephthalic acid plant wastewater in a microbial fuel cell," *Biotechnology Letters*, vol. 35, no. 2, pp. 197–203, 2013.

[39] L. Huang and B. E. Logan, "Electricity generation and treatment of paper recycling wastewater using a microbial fuel cell," *Applied Microbiology and Biotechnology*, vol. 80, no. 2, pp. 349–355, 2008.

[40] L. Huang, X. Yang, X. Quan, J. Chen, and F. Yang, "A microbial fuel cell–electro-oxidation system for coking wastewater treatment and bioelectricity generation," *J. Chem. Technol. Biotechnol.*vol. 85, no. 5, pp. 621–627, 2010.